RSC Advances

ROYAL SOCIETY OF CHEMISTRY

www.rsc.org/advances

Interface induced the transition from bipolar resistive switching to unipolar resistive switching in $Au/Ti/GaO_x/NiO_x/ITO$ structures

X. L. Chu [1], Z. P. Wu [1,2,a)], D. Y. Guo [1], Y. H. An [1], Y. Q. Huang [1], X. C. Guo [1], W. Cui [1], P. G. Li [1], L. H. Li [3], W. H. Tang[1,2,a)]

[1] Laboratory of Optoelectronics Materials and Devices, School of Science, Beijing University of Posts and Telecommunications, Beijing 100876, China

[2] State Key Laboratory of Information Photonics and Optical Communications, Beijing University of Posts and Telecommunications, Beijing 100876, China

[3] Department of Physics, The State University of New York at Potsdam, Potsdam, New York 13676-2294, USA.

a) Authors to whom all correspondence should be addressed. Electronic mail: zhenpingwu@bupt.edu.cn and whtang@bupt.edu.cn

Abstract

We report the transition from bipolar resistive switching (BRS) to unipolar resistive switching (URS) in the Au/Ti/GaO_x/NiO_x/ITO device at room temperature. After the proper soft breakdown of the p-n junctions (GaO_x/NiO_x), the switching operation could be easily transferred from BRS to URS mode. The BRS and URS behaviors are possibly related to the interfacial variation of the Ti/GaO_x Schottky junction barrier and GaO_x/NiO_x p-n junction barrier, respectively. The high/low resistance state can be distinguished clearly and be switched reversibly under a train of voltage pulses in both BRS and URS modes. The endurance characteristics show good reliability of the stored resistance state. These results suggest a potential device for the next generation of nonvolatile memory applications.

Introduction

Resistance changed by an external electric stimulus has attracted a great deal of attention for the application of resistive random access memory (RRAM). The advantages such as low power consumption, high speed operation, non-readout disturbance, and the high density integration potential make RRAM one of the most promising candidates for the next generation of nonvolatile memory.[1,2] Switching between the high resistance state (OFF) and the low resistance state (ON) in such systems involves either a bipolar RS (BRS) behavior or unipolar RS (URS) behavior based on the dependence of the applied electric polarity.[1,3,4] In general, there is only one switching type for a given RRAM device. Unipolar switching and bipolar switching have been widely observed in simple binary metal oxides such as NiO,[5] Cu_2O,[6] ZrO_2,[7] and TiO_2,[8] while generally only the bipolar switching is observed for complex perovskite-type oxide (ABO_3) films, such as PCMO,[9] Cr-doped $SrZrO_3$,[10] and $(Ba_{0.7}Sr_{0.3})TiO_3$.[11] Zheng *et al.*[12] also studied bipolar switching in a GaO_x-NiO_x p-n heterojunction. Both switching types have their own advantages. For example, the BRS offers more stable operation in terms of switching voltages and currents,[13,14] whereas the URS typically produces larger OFF/ON ratios and allows for a simple circuit architecture leading to higher integration density.[15,16] Hence, it would be advantageous to develop scalable material devices exhibiting both the bipolar and unipolar switching behaviors to expand the device application scope in nonvolatile memories. Recently, a signature for this has been observed in particular materials/devices. By increasing the forming current, Jeong *et al.* [17] successfully

obtained a transition from the BRS to the URS for the Pt/TiO_2/Pt sandwich structure that was originally known as a URS device. Following the same approaches as those of Jeong *et al.*, Sun *et al.* [18] and Shen *et al.* [19] studied the reversible transition between the BRS and URS for the Au/$SrTiO_3$/Pt and Pt/BST/Pt devices, respectively. Wei *et al.* [20] also studied the pulse-induced alternation from BRS to URS in the Ag/AgO_x/$Mg_{0.2}Zn_{0.8}O$/Pt device. In this article, we report the transition from BRS to URS in the Au/Ti/GaO_x/NiO_x/ITO device. Non-stoichiometric NiO_x ($x>1$) is a p-type semiconductor due to the excess oxygen ions as acceptors for generating holes[21] and non-stoichiometric GaO_x ($x<1.5$) is an n-type semiconductor due to the oxygen vacancies as donors for generating electrons.[22] Different from the previous work, the transition occurred in a multilayer structure with a p-n junction of GaO_x/NiO_x. The BRS is possibly induced by the migration of oxygen vacancies near the interfaces of Ti/GaO_x Schottky junction and the transition from BRS to URS is possibly induced by the proper soft breakdown of the p-n junctions (GaO_x/NiO_x). Moreover the high/low resistance state can be distinguished clearly and be switched reversibly under a train of voltage pulses in both BRS and URS modes.

Experimental

Commercial ITO glass was employed as the substrate and bottom electrode in our device. NiO_x thin film (210nm) was fabricated using radio frequency magnetron sputtering. A Ni disk was used as the target. The base pressure in the sputtering chamber was 1×10^{-4} Pa. The growth temperature and gas pressure ($Ar:O_2 = 2:1$) were fixed at 200 ^{o}C and 6×10^{-3} Torr, respectively. The as-grown NiO_x thin film is in

Ohmic contact with the ITO electrode, which is confirmed by the linear current-voltage (*I-V)* curve (Fig. 1(a)). Then, 550 nm-thick GaO_x thin film was grown on the NiO_x film by pulsed laser deposition technique under a vacuum environment of 1×10^{-6} Pa at room temperature. The laser ablation was carried out at the laser energy of 3 J/cm^2 with a repetition rate of 1 Hz using a KrF excimer laser (wavelength 248 nm). For electrical measurements, Au/Ti with a diameter of 200 μm was deposited on the GaO_x thin film by dc magnetron sputtering as the top electrode. Fig. 1(b) demonstrates the schematic diagram of the Au/Ti/GaO_x/NiO_x/ITO structure. The cross-sectional view of the structure is examined using field emission scanning electron microscopy (FE-SEM), as shown in Fig. 1(c). The switching characteristics and conduction mechanisms of the device were studied through *I-V* measurements using a Keithley 2450 source meter. The current from GaO_x to NiO_x was defined as the positive direction. All the measurements were carried out at room temperature.

Results and discussion

Fig. 2(a) plots the representative *I-V* characteristics of BRS behavior of the fresh memory device before the first soft breakdown. The initial resistance of the fresh device stays at the ON state. When the voltage sweeps from 0 V to 5.0 V (range 1) and then turns back (range 2), a hysteretic *I-V* curve is observed, which indicates that the device has been set to the OFF state. The device can be returned to the ON state by applying a negative bias (range 3 and 4). The above *I-V* curve of RS behavior is the typical BRS mode. The inset of Fig. 2(a) is the BRS performance over 20 cycles indicating a stable BRS behavior with good repeatability. To change the typical BRS

behavior to URS behavior, a high positive voltage is applied to the top electrode with a compliance current (I_{cc}) of 5 mA to avoid a complete dielectric breakdown. When the voltage increases further to + 6.2V, the soft breakdown occurs (the lower inset of Fig. 2(b)). The switching mode is transformed from BRS to URS. Fig. 2(b) plots the representative *I-V* characteristics of URS behavior. The memory cells were initially in OFF state. To switch the device to the ON state, a positive voltage of 3 V was applied to the top electrode with an I_{cc} of 5 mA. When a positive bias passes to a critical value of about 1.6 V, the current suddenly increases due to a restorable breakdown and the device is set from OFF to ON. An Ohmic behavior is observed. When the voltage was swept from 0 to 1 V with no compliance current, the current increased linearly with voltage and then dropped suddenly at a voltage of 0.53 V, indicating the abrupt increase in the resistance of the device. The device switched from ON into OFF state. The top inset of the Fig. 2(b) also shows the URS performance over 20 cycles, indicating good repeatability of the URS behavior.

For a memory device, it is important to investigate the statistical distribution of essential switching parameters. Fig. 2(c) and (d) show the cumulative probability data of the SET and RESET voltages for the BRS and URS modes respectively. The voltage values of the BRS behaviors are densely distributed. As for the URS behaviors, the transition voltages from the OFF to the ON state are distributed in a narrow range from 1.1 to 1.8 V. A small voltage range is required to minimize programming failure during the set process.

In order to realize the origin of the switching characteristics, the conduction

mechanisms responsible for the OFF and ON state are worth investigation. *I-V* curves of the device are replotted on a log-log scale. Fig. 3(a) shows the fitting results for the BRS under positive bias. The conduction behavior in the ON state represents Ohmic transport because the curve of the Log I – Log V is linear with a slope of about 1. However, the conduction mechanisms in the OFF state are much more complicated. Fitting results of the OFF state suggest that the current has a nonlinear dependence on voltage. At the lower voltage region, the $I - V$ curve exhibits linear behavior, the conduction is therefore governed by Ohmic law. The traditional nonlinear conduction mechanisms include space charge limited current (SCLC),[23,24] Schottky emission[25] and Poole-Frenkel (PF) emission.[19] It was found that the Schottky emission has the best fitting result in the present work. The linearity of LnI versus $V^{1/2}$ is shown in the inset of Fig. 3(a).

Fig. 3(b) demonstrates the fitting results for URS behavior under positive bias. For the ON state, the device exhibits Ohmic conduction behavior. The current depends linearly on the voltage with a slope of 1.0, indicating the existence of filamentary path.[26] However, for the OFF state, the case is more complicated. At the lower voltage region, the $I - V$ curve exhibits linear behavior, therefore the conduction behavior is governed by Ohmic law. With the increase of voltage, the current shows nonlinear dependence on voltage with a slope of about 1.6. And at higher voltage, a rapid current rise can be observed with a slope of 2.5. So, the SCLC has the best fitting result in the present work. We also find that the *I-V* curve has the shape of a bulge during the OFF state. After comparison, the Schottky emission fit better than

others. From the inset of Fig. 3(b), we can see that the linearity of LnI versus $V^{1/2}$ is good. It may be caused by the Schottky barrier at Ti/GaO_x interface. We will do further study and validation.

Switching in pulse mode for BRS and URS behavior is investigated to clarify the reliability of the device. For the BRS mode, a positive voltage pulse (0.2 s) of +5.0 V switches the system into the OFF state, as shown in Fig. 4(a). After applying a negative pulse (−3.0 V) of 0.2 s, the ON state is recovered. For the URS mode, a positive voltage pulse (0.2 s) of +3.0 V switches the system into the ON state. After applying a positive pulse (+1.0 V) of 0.2 s without compliance current, the "information" written to the device is erased and the OFF state is recovered, as shown in Fig. 4(b). For both BRS and URS mode, the readout voltage is +0.2 V, with a duration of 0.2 s for each voltage. The ON/OFF state can be distinguished clearly and be switched reversibly under a train of voltage pulses in both BRS and URS modes. The endurance measurements of the device demonstrate switching over 100 cycles. The resistance values of the two states are read out at +0.2V in each switching cycle. Fig. 4(c) and (d) respectively show the reliability of the stored resistance state of the two types of resistive switching modes. For the BRS behavior, the resistance ratio of HRS to LRS is about 5 and more importantly, the resistance values of each state are densely distributed. For the URS behavior, although the resistance values of HRS have a narrow range, the resistance ratio is about 10 which better than the BRS behavior. Both switching types have their own advantages.

The underlying mechanism of RS is still a controversial issue. However, there

exists a general agreement that both the filament and interface effect plays an important role. Akinaga *et al.* offered a unified model of RS based on such combination.[27] In order to understand the microscopic mechanism, a schematic energy band diagram of carrier transport under different applied electric fields is shown in Fig. 5. The mechanism for the BRS behavior is shown in Fig. 5(a) and 5(b). Under a positive voltage, the oxygen vacancies (near the interface of Ti/GaO_x) will move away from the anode (Fig. 5(a)).[28,29] Further increase of the positive bias leads to the suppression of oxygen vacancies at the interface of Ti/GaO_x,[23,30] resulting in an elevated Schottky barrier. Thus, a significant augment of effective barrier height could be expected, which brings the device from the ON to the OFF state. When a negative bias is applied to the top electrode, the oxygen vacancies will accumulate at the interface of the Ti/GaO_x. The effective barrier height will be reduced, leading to stabilization of the ON state. So the migration of oxygen vacancies causes the alteration of the Schottky barrier at the interface of the Ti/GaO_x, resulting in the BRS behavior. In the regime of BRS behavior, the oxygen vacancies (from inside GaO_x) and the oxygen ions (from inside NiO_x) do not assemble at the interfaces of GaO_x/NiO_x to form the the filamentary paths. After the first soft breakdown by a relatively larger bias, it is easier for the device to form the filamentary paths at the interfaces of GaO_x/NiO_x. Figs. 5(c) and (d) demonstrate the mechanism of the URS behavior. Under a positive forming voltage, the oxygen vacancies move toward the interface on the GaO_x side. Oxygen ions also accumulate at the interface on the NiO_x side. The oxygen ions and vacancies gather together to generate the filamentary paths

(Fig. 5(c)).[31] And the device switches to the ON state. Subsequently, the filament is ruptured by local excessive Joule heating due to the occurrence of high current density. The device switches to the OFF state. So, the formation and rupture of filamentary paths at the GaO_x/NiO_x result in the URS behavior.

Conclusions

In conclusion, BRS and URS behaviors have been observed in $Au/Ti/GaO_x/NiO_x/ITO$ structure. The switching operation could be easily transferred from the BRS to the URS mode after the proper soft breakdown of the p-n junctions (GaO_x/NiO_x). The ON and OFF state for both switching modes can be distinguished clearly and be switched reversibly under a train of voltage pulses. The underlying mechanism can be realized by the interfacial variation of the Ti/GaO_x Schottky junction barrier and GaO_x/NiO_x p-n junction barrier.

Acknowledgements

We thank Miss Liyuan Ji from Department of Chemistry, The state University of New York at Potsdam for taking part in this work during her summer vacation. This work was supported by the National Natural Science Foundation of China (51572033, 51172208, 61274017, 11404029), Beijing Natural Science Foundation (2154055), China Postdoctoral Science Foundation Funded Project (Grant No. 2014M550661), the Fundamental Research Funds for the Central Universities (Grant No. 2014RC0906), Fund of State Key Laboratory of Information Photonics and Optical Communications (BUPT).

References

1 R. Waser and M. Aono, *Nat. Mater.*, 2007, **6**, 833-840.

2 A. Sawa, *Mater. Today*, 2008, **11**, 28.

3 D. H. Kwon, K. M. Kim, J. H. Jang, J. M. Jeon, M. H. Lee, G. H. Kim, X. S. Li, G. S. Park, B. Lee, S. Han, M. Kim and C. S. Hwang, *Nat. Nanotechnol.*, 2010, **5**, 148-153.

4 D. L. Xu, Y. Xiong, M. H. Tang, B. W. Zeng and Y. G. Xiao, *Appl. Phys. Lett.*, 2014, **104**, 183501.

5 C. B. Lee, B. S. Kang, M. J. Lee, S. E. Ahn, G. Stefanovich, W. X. Xianyu, K. H. Kim, J. H. Hur, H. X. Yin, Y. Park and I. K. Yoo, *Appl. Phys. Lett.*, 2007, **91**, 082104.

6 A. Chen, S. Haddad, Y. C. Wu, Z. Lan, T. N. Fang and S. Kaza, *Appl. Phys. Lett.*, 2007, **91**, 123517.

7 C. Y. Lin, C. Y. Wu, T. C. Lee, F. L. Yang and C. Hu, *IEEE Electr. Device L.*, 2007, **28**, 366.

8 B. J. Choi, D. S. Jeong, S. K. Kim, C. Rohde, S. Choi, J. H. Oh, H. J. Kim, C. S. Hwang, K. Szot, R. Waser, B. Reichenberg and S. Tiedke, *J. Appl. Phys.*, 2005, **98**, 033715.

9 S. Q. Liu, N. J. Wu and A. Ignatiev, *Appl. Phys. Lett.*, 2000, **76**, 2749.

10 A. Beck, J. G. Bednorz, C. Gerber, C. Rossel and D. Widmer, *Appl. Phys. Lett.*, 2000, **77**, 139.

11 W. Shen, R. Dittmann, U. Breuer and R. Waser, *Appl. Phys. Lett.*, 2008, **93**,

222102.

12 K. Zheng, J. L. Zhao, X. W. Sun, V. Q. Vinh, K. S. Leck, R. Zhao, Y. G. Yeo, L. T. Law and K. L. Teo, *Appl. Phys. Lett.*, 2012, **101**, 143110.

13 M. J. Lee, C. B. Lee, D. Lee, S. R. Lee, M. Chang, J. H. Hur, Y. B. Kim, C. J. Kim, D. H. Seo, S. Seo, U. I. Chung, I. K. Yoo and K. Kim, *Nat. Mater.*, 2011, **10**, 625-630.

14 Y. Zhang, J. X. Shen, S. L. Wang, W. Shen, C. Cui, P. G. Li, B. Y. Chen and W. H. Tang, *Appl. Phys. A*, 2012, **109**, 219-222.

15 L. Goux, J. G. Lisoni, M. Jurczak, D. J. Wouters, L. Courtade and C. Muller, *J. Appl. Phys.*, 2010, **107**, 024512.

16 M. J. Lee, S. Han, S. H. Jeon, B. H. Park, B. S. Kang, S. E. Ahn, K. H. Kim, C. B. Lee, C. J. Kim, I. K. Yoo, D. H. Seo, X. S. Li, J. B. Park, J. H. Lee and Y. Park, *Nano Lett.*, 2009, **9**, 1476-1481.

17 D. S. Jeong, H. Schroeder and R. Waser, *Electrochem. Solid ST.*, 2007, **10**, G51.

18 X. W. Sun, G. Q. Li, X. A. Zhang, L. H. Ding and W. F. Zhang, *J. Phys. D: Appl. Phys.*, 2011, **44**, 125404.

19 W. Shen, R. Dittmann and R. Waser, *J. Appl. Phys.*, 2010, **107**, 094506.

20 L. L. Wei, J. Wang, Y. S. Chen, D. S. Shang, Z. G. Sun, B. G. Shen and J. R. Sun, *J. Phys. D: Appl. Phys.*, 2012, **45**, 425303.

21 K. Kinoshtia, T. Okutani, H. Tanaka, T. Hinoki, K. Yazawa, K. Ohmi and S. Kishida, *Appl. Phys. Lett.*, 2010, **96**, 143505.

22 L. Nagarajan, R. A. De Souza, D. Samuelis, I. Valov, A. Borger, J. Janek, K. D. Becker, P. C. Schmidt and M. Martin, *Nat. Mater*, 2008, **7**, 391.

23 D. Y. Guo, Z. P. Wu, L. J. Zhang, T. Yang, Q. R. Hu, M. Lei, P. G. Li, L. H. Li and W. H. Tang, *Appl. Phys. Lett.,* 2015, **107**, 032104.

24 M. H. Tang, Z. P. Wang, J. C. Li, Z. Q. Zeng, X. L. Xu, G. Y. Wang, L. B. Zhang, Y. G. Xiao, S. B. Yang and B. Jiang, *Semicond. Sci. Technol.,* 2011, **26,** 075019.

25 J. S. Choi, J. S. Kim, I. R. Hwang, S. H. Hong, S. H. Jeon, S. O. Kang, B. H. Park, D. C. Kim, M. J. Lee and S. Seo, *Appl. Phys. Lett.*, 2009, **95**, 022109.

26 R. Waser, R. Dittmann, G. Staikov and K. Szot, *Adv. Mater.*, 2009, **21**, 2632-2663.

27 H. Akinaga and H. Shima, *P. IEEE*, 2010, **98**, 2237-2251.

28 D. Y. Guo, Z. P. Wu, Y. H. An, X. C. Guo, X. L. Chu, C. L. Sun, L. H. Li, P. G. Li and W. H. Tang, *Appl. Phys. Lett.*, 2014, **105**. 023507.

29 D. Y. Guo, Z. P. Wu, Y. H. An,X. J. Li, X. C. Guo, X. L. Chu, C. L. Sun, M. Lei, L. H. Li, L. X. Cao, P. G. Li and W. H. Tang, *J. Mater. Chem. C*, 2015, **3**, 1830-1834.

30 D. Y. Guo, Z. P. Wu, P. G. Li, Y. H. An, P. C. Wang, X. L. Chu, X. C. Guo, Y. S. Zhi, M. Lei, L. H. Li and W. H. Tang, *Appl. Phys. Lett.*, 2015, **106**, 042105.

31 H. J. Zhang, X. P. Zhang, J. P. Shi, H. F. Tian and Y. G. Zhao, *Appl. Phys. Lett.*, 2009, **94**. 092111.

Figure and Table Captions

Fig. 1 (a) *I-V* curve of initial behavior in the ITO/NiO_x/ITO structure; (b) A schematic of the structure of the resistive switching device; (c) Cross-section SEM image of GaO_x/NiO_x structure.

Fig. 2 (a) Bipolar behavior in the Au/Ti/GaO_x/NiO_x/ITO structure, the inset shows the bipolar performance over 20 cycles; (b) Unipolar behavior in the Au/Ti/GaO_x/NiO_x/ITO structure, the top inset shows the unipolar performance over 20 cycles, the lower inset shows the first time of soft breakdown; (c) The voltage distributions for the SET and RESET of the BRS; (d) The voltage distributions for the SET and RESET of the URS.

Fig. 3 (a) *I-V* curves of the BRS under positive bias plotted on a log-log scale; (b) *I-V* curves of the URS under positive bias plotted on a log-log scale, the insets in both images show the Schottky emission fitting with $V^{1/2}$-Ln*I* axes.

Fig. 4 (a) BRS behavior under a train of voltage pulses; (b) URS behavior under a train of voltage pulses; (c) The resistance distribution of HRS and LRS in 100 cycles of the BRS; (d) The resistance distribution of HRS and LRS in 100 cycles of the URS.

Fig. 5 Schematic diagram for the microscopic mechanism of the resistance switching.

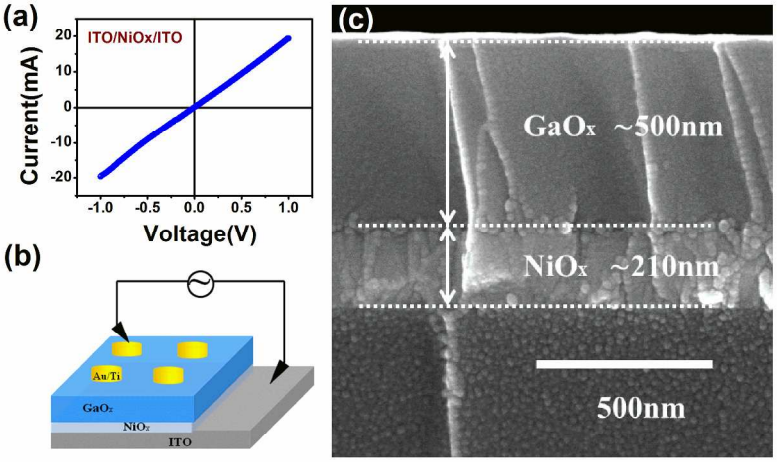

296x210mm (300 x 300 DPI)

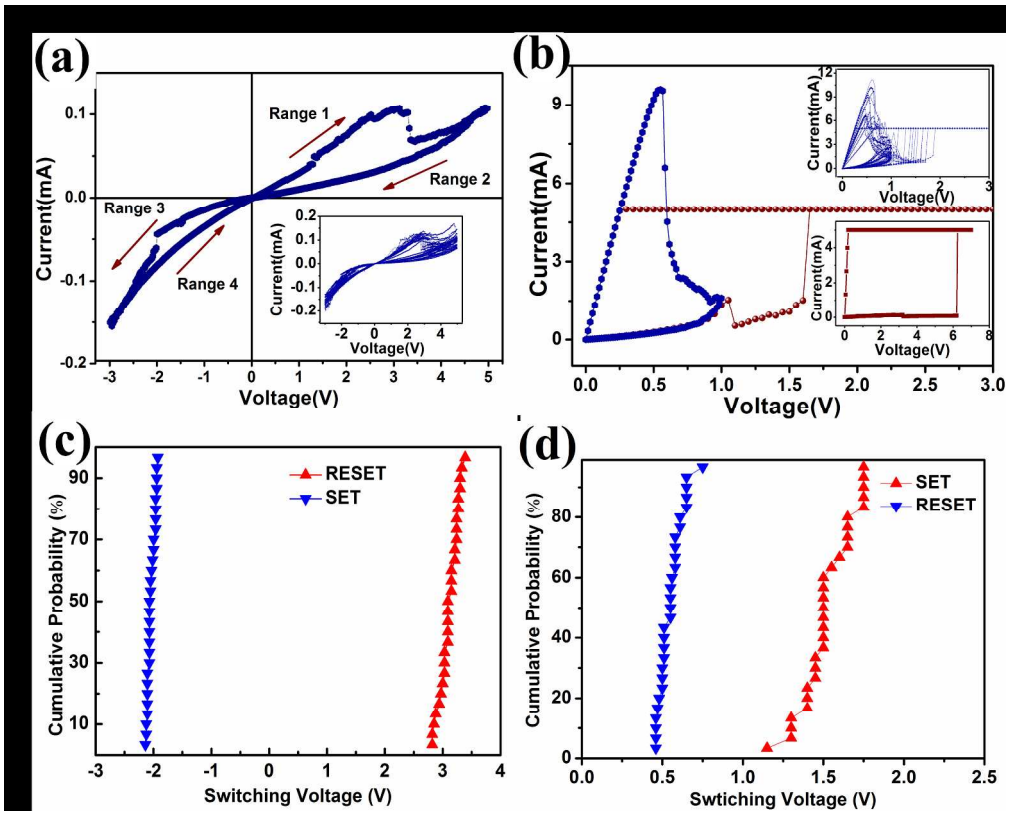

517x416mm (150 x 150 DPI)

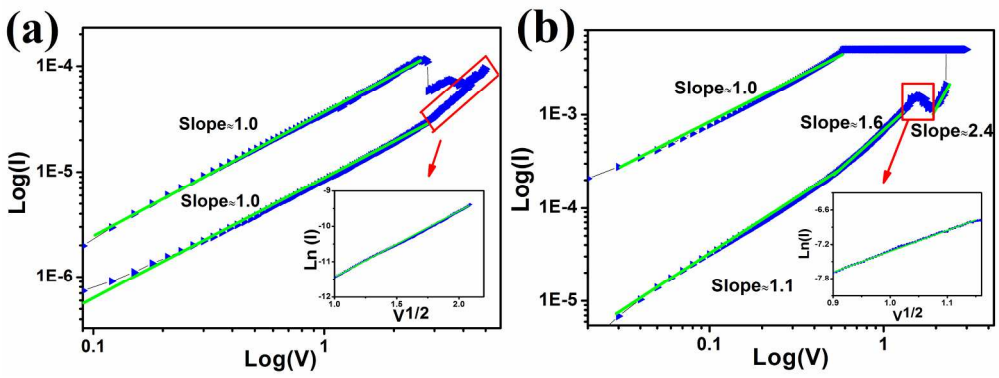

447x169mm (150 x 150 DPI)

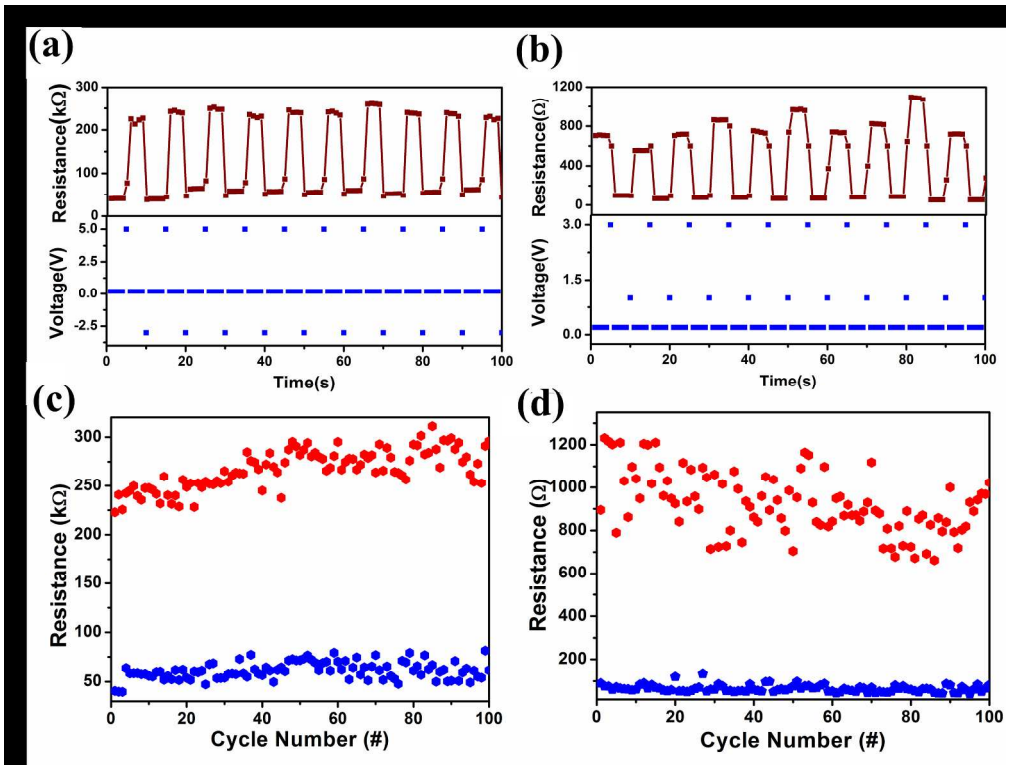

483x367mm (150 x 150 DPI)

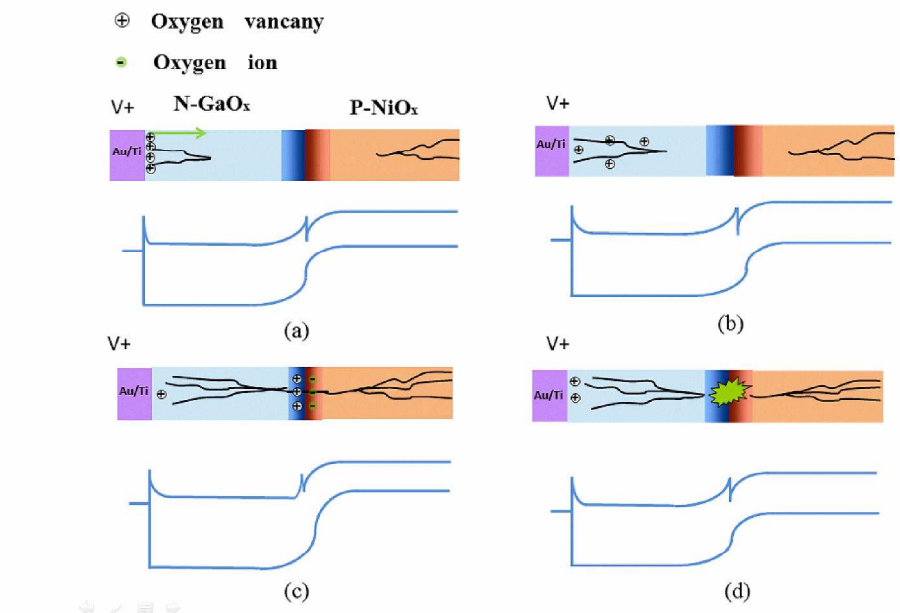

287x201mm (300 x 300 DPI)

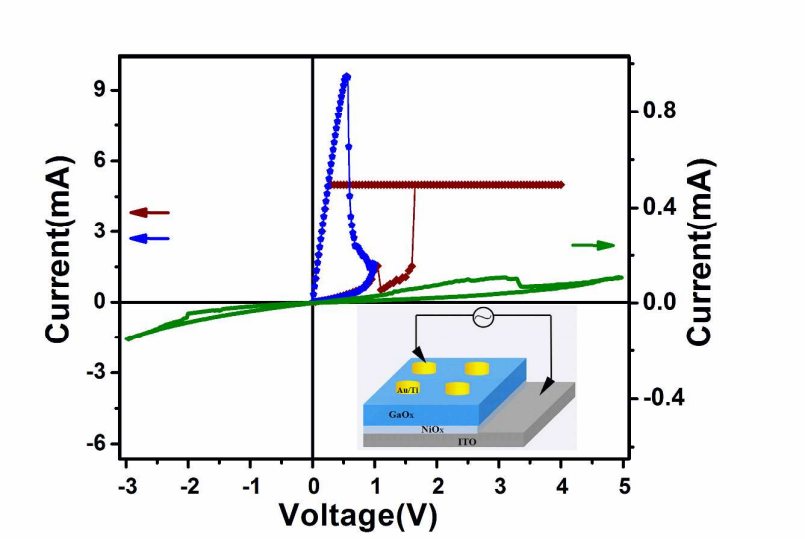

The transition of resistive switching behavior from bipolar to unipolar induced by interface was found and investigated in Au/Ti/GaO_x/NiO_x/ITO structure.